**PAPER**

# Flow quantization and nonequilibrium nucleation of soft crystals

Arash Nikoubashman,*[a] Gerhard Kahl[a] and Christos N. Likos[b]

We consider dense systems consisting of ultrasoft, overlapping particles under shear and transport flow, by employing a multiscale simulational approach that combines multiparticle-collision dynamics for the solvent particles with standard molecular dynamics for the solute. We find that the nucleation rates of supercooled liquids can be dramatically accelerated *via* the shear-induced formation of an intermediate string pattern, which disaggregates after the cessation of shear, leading to the emergence of three-dimensional fcc order. Furthermore we expose these cluster crystals to Poiseuille flow and we establish the emergence of a quantized flow pattern, in which both the height and the width of the fluid stream display well-defined plateaus as a function of the applied pressure gradient. The resulting velocity profiles of the solvent closely resemble plug flow. We explain the emergence of the plateaus by successive fluidization of crystalline layers adjacent to the channel walls and discuss the dependence of the discrete flow on the cluster aggregation parameter. Cluster crystals thus emerge as novel systems with applications on nano- and microfluidic devices, allowing the manipulation of flow in a precisely controlled way.

## I. Introduction

Colloidal dispersions and polymer solutions confront fundamental research with a formidable challenge due to the fact that they are *non-Newtonian* fluids. Consequently, they offer a wide spectrum of possibilities in rheological applications. Contrary to simple liquids, their viscosity depends on the applied external stresses, such as shear, pressure gradients or other fields. A key role in their rheology is played by the presence of at least two components, the solvent and the suspended particles, with vastly disparate length- and time-scales. In the case of polymer solutions, entanglements between the chains are an additional feature with very important dynamical consequences. The flow properties of complex fluids become even more relevant in the modern fields of micro- and nanofluidics, where the narrow geometrical constrictions of the confining channels bring forward novel properties and highlight the effects of the coupling to the surrounding walls. Some of the most prominent and widely-discussed rheological properties of non-Newtonian liquids include shear-banding,[1] thixotropy,[2] shear-thinning[3,4] as well as shear-thickening.[3] Such complex fluids are also relevant for a wide variety of applications in nanotechnology and micro-patterning,[5,6] in microfluidics,[7] shock absorption,[8] and protective clothing.[9] In addition, they are also encountered in many biological systems, *e.g.* in cytoplasm and blood.

The relation between the microscopic interactions between the particles and the macroscopic shear-flow properties of such liquids has been a subject of vast interest in the last decades, and considerable research has been already devoted to colloidal suspensions that consist of both hard[10,11] and charged colloids.[12,13] Shear often acts in a way that suppresses spatial order: shearing a crystal can gradually reduce the three-dimensional periodicity of the same, bringing about a shear-induced disorder transition to a uniform phase. On the other hand, steady shear can have the opposite effects on thermodynamically metastable fluids. The latter are uniform phases that are separated by their equilibrium, crystalline phase by a sufficiently high nucleation barrier, so that they either remain supercooled for macroscopically long times or get trapped into a glassy state. A characteristic example is the dynamical arrest of soft colloids, such as star polymers or star-like micelles,[14–18] which takes place in regions of the phase diagram that correspond to an equilibrium face centered cubic (fcc) crystal. Shear can induce three-dimensional periodicity to such a supercooled or arrested solution, accelerating thereby the nucleation rates in metastable liquids after the cessation of shear. This shear-induced crystallization has been demonstrated convincingly for soft colloids, and in particular for block copolymer micelles, in the seminal work of Mortensen, Brown, and Nordén.[19]

In addition to shear, another prominent prototype of non-equilibrium processes is transport flow along channels, driven by a pressure gradient. Here, complex fluids are of particular technological importance because the control of their flow properties has numerous applications. Characteristic examples are the directed assembly of mesoscale periodic structures,[20–23] the

*[a]Institute of Theoretical Physics and CMS, Vienna University of Technology, Wiedner Hauptstraße 8-10, A-1040 Vienna, Austria. E-mail: arash.nikoubashman@tuwien.ac.at*
*[b]Faculty of Physics, University of Vienna, Boltzmanngasse 5, A-1090 Vienna, Austria*

controlled synthesis and manipulation of monodisperse, soft colloidal particles,[24–28] the measurement of the elastic properties of the same,[29] as well as the manufacturing of specific nanofluidic devices such as nanopumps[30] or moving-wall channels.[31] On the more fundamental side, recent research activity has focused on the transport flow of colloidal gels[32–34] and of concentrated colloidal dispersions close to their jamming point,[35–40] as well as on the related issue of flow and filtration of Brownian colloidal or non-Brownian, wet granular matter.[41–44]

In this paper, we study the behavior of ultrasoft colloids under shear and transport flow. The interaction potential of these particles is *bounded*, thus allowing full and multiple particle overlap. Though surprising and unphysical at first glance, this condition is fully legitimate and natural for fractal, polymer-based colloids, such as amphiphilic dendrimers[45] and unknotted ring polymers.[46] The peculiar property of this class of particles is that they can form stable cluster crystals where each lattice site is occupied by an accumulation of $N_c$ particles.[47–49] A necessary and sufficient prerequisite for the emergence and stability of these crystals is the existence of negative components in the Fourier spectrum of the interaction potential.[50,51] Furthermore, the position of this minimum dictates the lattice constant $a$ of the crystal, rendering it essentially density-independent. The immediate consequence of this fact is that $N_c$ scales proportionally to the density $\rho$, leading to highly unusual equilibrium dynamics, namely a superposition of phononic oscillations[52] and activated hopping dynamics.[53,54] While the *equilibrium* properties of these novel structures have been studied thoroughly by now, only little was known about their response to external drive until most recently.[55]

Using a simulation technique that explicitly takes into account the solvent, we established in ref. 55 that cluster crystals respond to shear through the formation of strings, which are arranged hexagonally in the gradient-vorticity plane. In the present contribution we provide evidence that this dynamical transition to a two-dimensional modulated state can be exploited to accelerate the crystallization rates of supercooled liquids dramatically: after the cessation of shear, particles arranged along a string break up in distinct clusters, leading to the emergence of three-dimensional order. Going further, we investigate how the cluster crystal is affected by transport flow. To this end, we have carried out computer simulations, where fcc cluster crystals with three different occupation numbers $N_c$ were placed into a channel and exposed to Poiseuille flow along the crystallographic [100] and [111] direction. From our simulations we find that the presence of the crystal drastically affects the flow pattern of the dispersion, *i.e.* resulting into a pronounced flattening of the usually parabolic shape, and thus bringing about what is known in literature as *plug flow*. In those regions of the channel where the velocity profile is essentially flat, the solvent flows with almost constant velocity and the structural integrity of the whole lattice is preserved (aside from a weak distortion). Close to the walls however, where the velocity profile is almost linear, the crystal liquefies. Moreover, we discover that the flow becomes *quantized* as the pressure drop along the channel is increased. The flow-profile *vs.* pressure curves display broad plateaus with sudden jumps among them, each corresponding to the melting of two additional layers of the remaining cluster crystal slab which flows with constant velocity in the center of the channel. The width of the flat part of the velocity profile shows a similar evolution, following successive.

The whole process is accompanied by a small but sizable wall-slip. This behavior bears on one hand some similarities to the flow of concentrated colloidal suspensions or gels but on the other hand has also significant differences, which render the cluster crystals unique among complex fluids in their transport flow behavior, as it will be discussed in the following.

The rest of this paper is organized as follows. In Sec. II we present our model and simulation method. Our results concerning the shear induced crystallization are presented and discussed in Sec. III, and the ones pertaining to the transport flow in Sec. IV. Finally, we summarize the findings and draw our conclusions in Sec. V.

## II.   Model and simulation method

In this work, we studied the effects of shear on crystallization in supercooled liquids through shear-induced ordering, as well as the impact of transport flow on a face-centered cubic cluster crystal consisting of soft, overlapping particles. The interaction potential between the solute particles is given by the generalized exponential model with exponent 8 (GEM-8) potential:

$$U(r) = \varepsilon \exp[-(r/\sigma)^8], \quad (1)$$

with $\varepsilon$ and $\sigma$ setting the units of energy and length, respectively. Based on general arguments we expect, however, our results to be valid for all potentials in the $Q^{\pm}$-class.[47,50,55] The sheared systems, employed to analyze the effects of shear on crystal nucleation, were supercooled uniform fluids. Stable, initially ordered systems, on the other hand, were placed inside a microscopic solvent which, in the absence of the solutes, was flowing under Poiseuille flow. The GEM-8 crystals were oriented along either the crystallographic [100] or the [111] plane at temperature $k_B T/\varepsilon = 0.2$. Thereby, the (100) surface is obtained by cutting the crystal parallel to the front surface of the fcc cubic unit cell, leading to an arrangement of four-fold symmetry; the (111) surface is obtained by slicing the crystal in such a way that the surface plane intersects the $x$-, $y$- and $z$-axes at the same value, resulting in a particle arrangement of six-fold symmetry. All simulations have been carried out in a cubic simulation box at three different state points with $\rho\sigma^3 = 2.6$, 3.9, and 5.9 (corresponding to average cluster occupation numbers $N_c = 4$, 6, and 9 of the equilibrium crystals, respectively). As shown in Fig. 1, the system forms stable fcc cluster crystals in the (constrained) bulk phase at these state points.[56]

The walls were separated by a distance $L_x = 11\sigma$ along the gradient ($x$) direction, and the interaction between the solute particle and the wall was chosen to be given by the soft and steep potential:[57]

$$U_{\text{wall}}(x) = \begin{cases} \dfrac{2}{3}\pi\varepsilon\left[\dfrac{2}{15}\left(\dfrac{\sigma}{x}\right)^9 - \left(\dfrac{\sigma}{x}\right)^3 + \dfrac{\sqrt{10}}{3}\right], & 0 \le x \le (2/5)^{1/6}\sigma \\ 0, & x > (2/5)^{1/6}\sigma. \end{cases}$$

$$(2)$$

Thereby, the total external potential caused by both walls is given by $U_{\text{ext}}(x) = U_{\text{wall}}(x) + U_{\text{wall}}(L_x - x)$. Additionally, we have employed no-slip boundary conditions for the solvent particles along this direction, and periodic boundary conditions
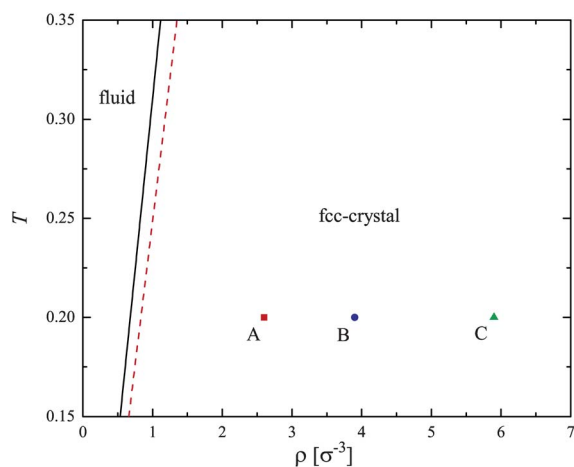
**Fig. 1** The (constrained) bulk phase diagram for the GEM-8 particles in ($\rho$, T)-plane.[56] Lines show the phase boundaries for the liquid (solid black) and the fcc phase (dashed red). The gap in-between denotes the coexistence region. Symbols show the investigated state points.

in the vorticity ($y$) and flow ($z$) direction for both the solvent and the solute. The geometry of this setup and the different flow patterns generated for the pure solvent (see below) are schematically illustrated in Fig. 2.

In order to incorporate hydrodynamic interactions (HI) as faithfully as computationally feasible, we have opted to employ a hybrid simulation approach, in which standard molecular dynamics (MD) algorithms are combined with the Multi-Particle Collision Dynamics (MPCD) simulation technique.[58,59] This choice is motivated by the large disparities in the length and time scales, characteristic for the solvent molecules and the embedded particles, which makes atomistic simulation studies prohibitively time-consuming. Hydrodynamics play not only an important role for the non-equilibrium behavior of the cluster crystal, but also for the equilibrium dynamics, as the solvent significantly affects the particle hopping.[60]

MPCD is a mesoscopic, particle-based simulation method, consisting of alternating *streaming* and *collision* steps, where the solvent particles are assumed to be non-interacting. Instead, the coupling between the solvent and solute particles is realized through momentum exchange during the collision step.[61] During the streaming step, the solvent particles of unit mass $m'$ propagate ballistically over a period of $\Delta t$:

$$\mathbf{r}_i'(t + \Delta t) = \mathbf{r}_i'(t) + \Delta t \mathbf{v}_i'(t), \tag{3}$$
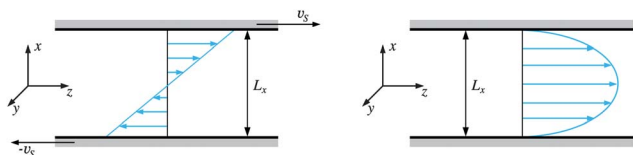


**Fig. 2** Schematic representation of the simulation setup, demonstrating the flow ($z$), gradient ($x$), and vorticity ($y$) directions. The left panel shows the shear flow, while the right panel shows the Poiseuille flow for the pure solvent.

where $\mathbf{r}_i'(t)$ is the position and $\mathbf{v}_i'(t)$ the velocity of this solvent particle at time $t$. In the collision step, the solvent and solute particles, grouped into cells, undergo stochastic collisions with particles within the same cell:

$$\mathbf{v}_i'(t + \Delta t) = \mathbf{u}_j(t) + \Omega(\alpha)[\mathbf{v}_i'(t) - \mathbf{u}_j(t)], \tag{4}$$

with $\mathbf{u}_j$ denoting the center of mass velocity of the $j$-th collision cell, and $\Omega$ being a norm-conserving rotation matrix around a fixed angle $\alpha$. The size of these collision cells determines the spatial resolution of the HI, and we have opted for an edge length of $\sigma$. The mean free path of a solvent particle is then given by $\lambda \sim \Delta t \sqrt{T}$, and it has been shown in ref. 62 that Galilean invariance is violated for $\lambda < \sigma/2$. Therefore, all lattice cells are shifted by a randomly chosen vector, drawn from a cube with edge length in the interval $[-\sigma/2, +\sigma/2]$ before each collision step. Whereas the above-described rules governing the solvent dynamics are general, the simulation of specific flow profiles requires special care and will be discussed in what follows.

Shear flow with shear-rate $\dot{\gamma} = 2v_S/L_x$ was incorporated into the system by rescaling the center of mass velocities of the collision cells close by the shear plane to $\pm v_S$.[63] We have favored this approach over other methods (such as the Lees–Edwards boundary conditions[64]), since the employed boundary conditions resemble more the actual experiment and lead to a spontaneous development of the desired linear velocity profile. Since in our approach the velocity profile is *not* externally imposed, but completely self-emerging, we can also observe phenomena such as wall-slip, nonlinear velocity, or density profiles. In addition, shearing only the fluid and not the colloidal dispersion as a whole works as well for dilute dispersions,[65,66] but for dense systems, this approach is not suitable since the resulting viscosity is much too small.[67]

Poiseuille flow is driven by a pressure gradient parallel to the flow direction, and is slowed down by viscous drag along both plates, so that these forces are in balance. Several methods exist for generating such a flow, for instance forced,[58,68,69] surface-induced, and gravitational[70,71] approaches. We adopted the latter technique in our simulations, since the other two techniques produce a considerable distortion of the velocity-field and density profile along the flow direction.[70] The external force acting on the unit volume of the fluid, $\mathcal{F}$, is given by $\mathcal{F} = \varrho_s g \hat{\mathbf{z}}$, where $\varrho_s$ is the mass density of the solvent and $g$ is the acceleration constant. The effect of $\mathcal{F}$ can easily be incorporated into the streaming step as follows:

$$\mathbf{r}_i'(t + \Delta t) = \mathbf{r}_i'(t) + \Delta t \mathbf{v}_i'(t) + \frac{\Delta t^2}{2} g \hat{\mathbf{z}}; \tag{5}$$

$$\mathbf{v}_i'(t + \Delta t) = \mathbf{v}_i'(t) + \Delta t g \hat{\mathbf{z}}. \tag{6}$$

The strength of the gravitational field can be varied by tuning $g$, and a steady Poiseuille flow builds up self-consistently after a short time when no-slip boundary conditions are applied at the surface layers. For planar walls coinciding with the boundaries, such conditions are conveniently simulated by employing a bounce-back rule, *i.e.*, the velocities of particles that hit the walls are inverted after the collision. However, for a more general setup the walls will not coincide with, or even be parallel to the cell boundaries. Furthermore, partially occupied cells can also

emerge from the cell-shifting, which is unavoidable for small mean free paths $\lambda$. Lamura et al. have demonstrated that the bounce-back rule has to be modified in such a case, by refilling of boundary cells with virtual particles;[69] this feature has been included in our implementation.

Additionally, thermostatting is required in any non-equilibrium MPCD simulation whenever either isothermal conditions are required or viscous heating can occur. The thermostat employed was based on rescaling the random part of the velocities to maintain constant temperature.[65] The MPCD parameters employed were $\alpha = 130$, $\lambda = 0.1$, with 30 solvent particles per collision cell. Solute particles of mass $m = 5m'$ each were coupled to the solvent via participation to the MPCD collision step, while at the same time the GEM-8 direct interactions between the same were taken into account in a conventional MD approach. For the conventional MD-step, we employed a Verlet integration scheme with $\Delta t_{\mathrm{MD}} = 2 \times 10^{-3}$, whereas the MPCD time step was $\Delta t = 10^{-1}$, measured in the unit of time $\tau = \sqrt{m' \sigma^2 / \varepsilon}$.
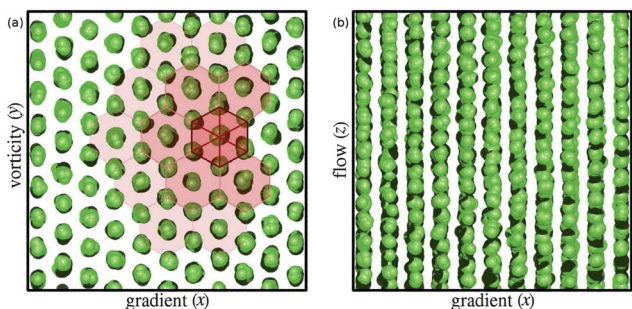
## III. Shear-induced crystallization

We first studied the possibility of accelerating the nucleation rates in undercooled liquids through shear. The question of whether steady shear facilitates[19] or suppresses[72] the nucleation of a crystal from the metastable melt is a longstanding debate, and it seems that the answer is not universal, it is, strongly system dependent. For soft colloids, such as copolymer micelles, experimental evidence supports the acceleration of nucleation due to shear. There is, however, a particularity that makes the whole family of $Q^{\pm}$-interaction potentials distinct, namely the way in which dense solutions of such particles self-organize under shear. In ref. 55, we have shown that the application of steady shear leads, at low shear-rates, to shear-banding, followed by string formation, in which the flow-aligned strings form a hexagonal lattice on the gradient-vorticity plane (see Fig. 3). As the shear-rate further increases and eventually exceeds a well defined critical shear-rate $\dot{\gamma}_c \propto \sqrt{\rho}$, the string phase melts into a uniform, disordered fluid with an accompanied increase of the viscosity. At high shear rates, hydrodynamic interactions play a particularly important role, since they dramatically facilitate the breakup of strings. Since these strings formed out of both



**Fig. 3** (a) Vorticity–gradient and (b) flow–gradient views of the strings formed in an cluster crystal with $N_c = 9$ under shear with a shear-rate $\dot{\gamma} = 0.2$. Green spheres (not drawn to scale) represent GEM particles. In panel (a), a few centers of mass of the strings are connected by straight lines, the red shading of the resulting hexagonal tiles reflects the distance from the arbitrarily chosen central string.

crystals and supercooled fluids, shear provides a way to reduce the spatial symmetry, bringing thus the system closer to full, three-dimensional broken translational invariance. This property opens up a unique pathway to possible nucleation, since it offers the system the possibility to augment its departure from full translational symmetry in a stepwise fashion, a possibility that is not present for hard colloids.

To investigate these questions, we thus applied the following shear-protocol: We considered supercooled fluids at the state points A, B, C (see Fig. 1), and sheared them for a period of $\tau_{\mathrm{shear}} = 500$. The shear computer experiments are conducted with $\dot{\gamma} = 0.2$, resulting into spontaneous string formation.[55] Systems that have been prepared in this way are henceforward referred to as presheared. After the strings have emerged, we turned off the shear-flow and left the system to rest (total simulation time $\tau_{\mathrm{sim}} = 10000$). Then we analyzed the equilibrated structures, and compared them with those of unsheared, confined fluids of equal density and temperature, by calculating the free volume fraction $\Phi$, the averaged bond order parameters,[73,74] and the one-particle density distributions of the equilibrated final structures.

For the calculation of $\Phi$, we considered each GEM-particle as a sphere of diameter $\sigma$ and calculated the free volume in each state by straightforward counting. The identification of bond order parameters as a measure for local crystalline ordering in liquids and glasses was originally introduced by Steinhardt et al.[73] and then refined in ref. 74. We followed the latter scheme, and calculated the averaged local bond order parameters $\bar{Q}_4$ and $\bar{Q}_6$. Here, we first identified the clusters along the lines of ref. 54, and then determined the parameters for the ideal fcc structure ($\overline{Q}_4^{\mathrm{fcc}} = 0.135 \pm 0.003$ and $\overline{Q}_6^{\mathrm{fcc}} = 0.264 \pm 0.004$) and for the uniform liquid state ($\overline{Q}_4^{\mathrm{liq}} = 0.110 \pm 0.003$ and $\overline{Q}_6^{\mathrm{liq}} = 0.125 \pm 0.003$). Finally we calculated the values of $\bar{Q}_4$ and $\bar{Q}_6$ for the presheared and unsheared systems and compared them with our reference values. In what follows, all results are shown for the [100]-orientation (unless explicitly stated otherwise), since the orientational dependence is very weak.

The results for the free volume fraction and for the bond-order parameters are shown in Table 1, and at a first glance, no effect of the different treatment is observable. However, we have to keep in mind that the bond order parameters are a measure for the averaged local crystalline order, and give only limited information about the global ordering of the system. Evidently, a more appropriate measure of long-range order is called for, and this is offered by the averaged one-particle density $\rho(\mathbf{r})$ of the system. Indeed, and following also the terminology of ref. 56, we term a system as fluid for which the one-particle density has the same

**Table 1** Free volume fraction $\Phi$ and bond order parameters $\bar{Q}_4$ and $\bar{Q}_6$ for the presheared and unsheared system

| $N_c$ | $\Phi$ | $\bar{Q}_4$ | $\bar{Q}_6$ |
|---|---|---|---|
| 4 (presheared) | 0.496 | 0.098 | 0.267 |
| 4 (unsheared) | 0.494 | 0.101 | 0.268 |
| 6 (presheared) | 0.506 | 0.094 | 0.252 |
| 6 (unsheared) | 0.508 | 0.098 | 0.260 |
| 9 (presheared) | 0.511 | 0.109 | 0.262 |
| 9 (unsheared) | 0.512 | 0.110 | 0.254 |

symmetry as the underlying Hamiltonian, and as a crystal one in which translational symmetry is broken in a periodic fashion. Accordingly, systems for which $\rho(\mathbf{r}) = \rho(x)$ only, are supercooled confined fluids, whereas if a density profile depending on all three spatial coordinates, $\rho(x, y, z)$, results, we talk about a solid. Naturally, in the latter case, spatial periodicity in the $y$- and $z$-directions compatible with the fcc-crystal must also be present, whereas in the $x$-direction only a finite number of fcc elementary cells can be present.

Employing this criterion, a remarkable difference between the presheared and the unsheared systems emerges, as can be seen in Fig. 4 and 5: while the unsheared systems show spatial modulation only in the $x$-direction, the lattice sites in the presheared systems are very well separated from each other, and the latter easily find their way to crystallization after shear. This distinction is most pronounced for the system with the lowest density ($\rho = 2.6$), but disappears completely for the densest one ($\rho = 5.9$), since the nucleation barrier decreases as $\rho$ grows, and thus preshearing is not necessary to accelerate crystallization anymore.

It can hence be argued that, for the $Q^{\pm}$-systems, shear has a profound effect in bringing about an effective lowering of the nucleation barrier, thereby accelerating the crystallization rates. This happens through a particular dynamical pathway that involves first the breaking of the symmetry in the gradient- and vorticity-directions through the formation of a two-dimensional triangular lattice of strings, which then proceeds to relaxing towards a crystal after the cessation of shear. The physical reason behind this pathway rests, again, on the particular property of these systems to have an hidden propensity to an instability towards spatial modulation with wavenumber $Q_*$, where $Q_*$ is the position of the negative minimum of the Fourier transform of the interaction potential.[47,50] Whereas in the unsheared system this instability is not sufficient to drive immediate crystallization, and the fluid can thus remain trapped in a metastable phase for long times, once shear has been applied, spatial modulation in two dimensions takes place as the result of the external drive. Along the flow direction, the strings have liquid-like ordering, which is, however, only sustainable as long as shear is on.[55] Once the latter ceases, the liquid-like strings are not anymore stable, and the existing two-dimensional order offers an effective 'substrate' on which the particles along the string now perform an essentially one-dimensional nucleation, clumping into clusters and building up the thermodynamically stable crystal. Naturally, the deeper we go into the region of stability of the solid, the less the effect of shear, since nucleation barriers decrease as the distance from the crystallization point grows.

## IV. Transport flow

### A. Flow profiles and crystal transport

In the second part of our analysis, we have studied the impact of Poiseuille flow by conducting a series of simulations for different occupation numbers $N_c$ and crystallographic orientations. The strength of the flow has been varied through the gravitational constant $g \in [0, 0.1]$, which induces a pressure drop along the channel. Performing the MPCD-simulations as described in Sec. II, and in particular under the collision rules of eqn (5) and (6), the pure solvent inside the channel of width $L_x$ develops the Hagen–Poiseuille velocity profile:

$$v_z^{(0)}(x) = \frac{\varrho_s g}{2\eta}(L_x - x)x, \tag{7}$$

where the superscript denotes the fact that this is the velocity profile of the *pure solvent*, as opposed to the one when solute particles are present. In eqn (7) above, the solvent viscosity $\eta$ is determined by the solvent mass density $\varrho_s$ and the collision rules, *i.e.*, it is not an input parameter to the simulation. The parabolic velocity profile vanishes at $x = 0$ and at $x = L_x$, and attains its maximum value, $v_0$, at the middle of the channel ($x = L_x/2$), *viz.*:

$$v_0 = \frac{\varrho_s g L_x^2}{8\eta}. \tag{8}$$

Eqn (7) further implies that a local shear rate $\dot{\gamma}^{(0)}(x) = \partial v_z^{(0)}(x)/\partial x$ is established in the fluid, expressed as:
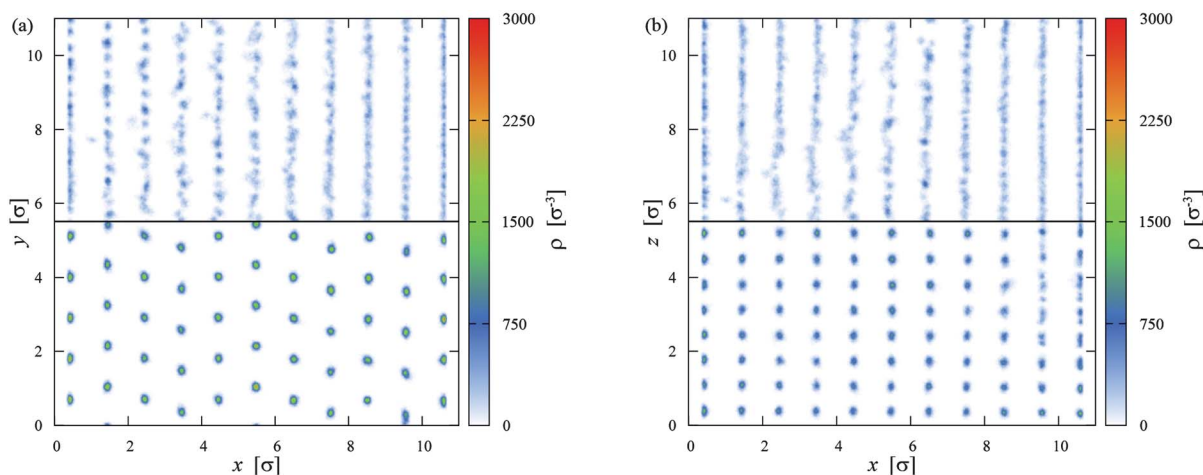


**Fig. 4** Two-dimensional color coded density profiles for $\rho = 3.9$. The left panel shows the distribution in the gradient–vorticity plane, while the right panel shows the data in the gradient–flow plane. The top half of each image shows the unsheared system, while the lower half shows the presheared system (after cessation of shear).
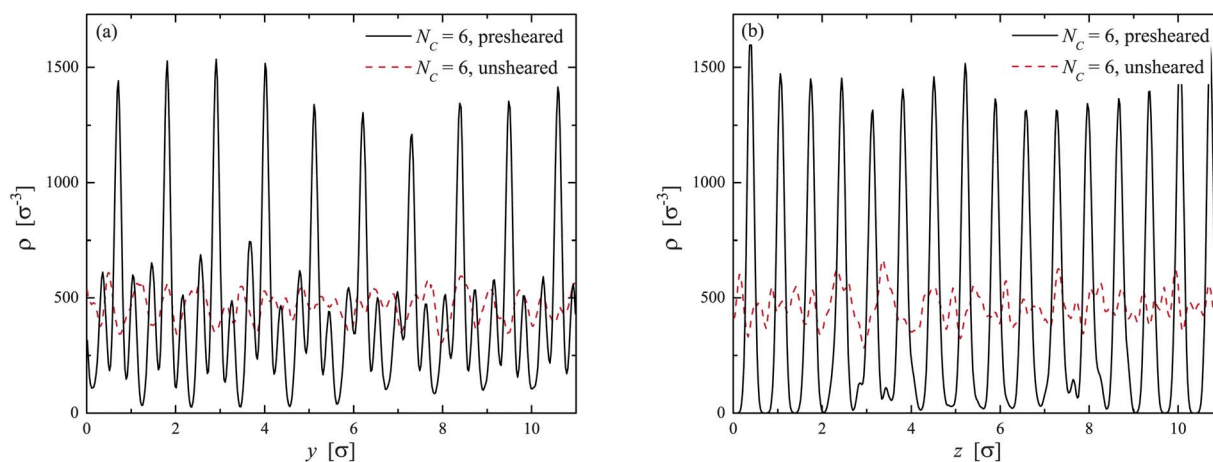
**Fig. 5** Density profiles for $\rho = 3.9$ along the vorticity ($y$) and flow ($z$) direction. Continuous lines show results for the presheared setup, while dashed lines represent the unsheared systems.

$$\dot{\gamma}^{(0)}(x) = \frac{\varrho_s g}{2\eta}(L_x - 2x). \qquad (9)$$

Before proceeding to a detailed description of the results of our numerical experiment, it is worth anticipating on a *qualitative level* the behavior of the cluster crystal and of the solvent under these conditions, on the basis of previously-known results and physical argumentation. Suppose first that the external pressure gradient is strong enough, so that the inserted cluster crystal (which is hydrodynamically coupled to the fluid) can be treated as a perturbation, *i.e.*, let us assume that the solvent velocity profile given by eqn (7) above remains essentially unaffected by the solute. This implies that the latter is locally exposed to shear rates given by eqn (9). Based on previous work,[55] we know that cluster crystals under shear react by forming strings that are aligned along the flow ($z$) direction and they self-assemble on a triangular lattice on the gradient–vorticity plane. Accordingly, one could argue that such strings also form under Poiseuille flow conditions. However, as can be seen from eqn (9), the shear rate at the center of the channel vanishes. Given the fact that a small but finite shear rate is necessary for the formation of strings,[55] this local analysis would imply that there are a few (and, at any rate, at least one) crystalline layer(s) in the middle of the channel, lying perpendicular to the gradient direction (*i.e.*, on the flow–vorticity plane), which do not melt. Instead, they remain intact in their crystallinity, and they are simply driven along by the fluid flow. However, this scenario of simultaneous presence of two-dimensional crystalline layers drifting on the ($y$, $z$)-plane and of parallel strings oriented along the $z$-axis is untenable. Indeed, in such a case, the crystalline layers would act on the neighboring strings, immediately close to them along the gradient direction, as external potentials. Since the relative velocities $v_{rel}$ of particles displaced along the gradient direction are non-vanishing, these external potentials would feature periodic, spatiotemporal modulation along the flow-direction. The potential acting on the strings would thus have the form of some function $f(z - v_{rel}t)$, whose explicit expression depends on the interparticle interaction, spacing, and cluster occupancy $N_c$ but it is

otherwise irrelevant for the rest of the argument. However, under the action of such an external potential, the strings would no longer be able to maintain their spatial uniformity along the $z$-direction, and they would break up into clumps (see the discussion on the acceleration of the nucleation rates in the preceding Section). Such a breakup would then act as an additional external potential to the next neighboring strings, with the result that they would also break up and so on.
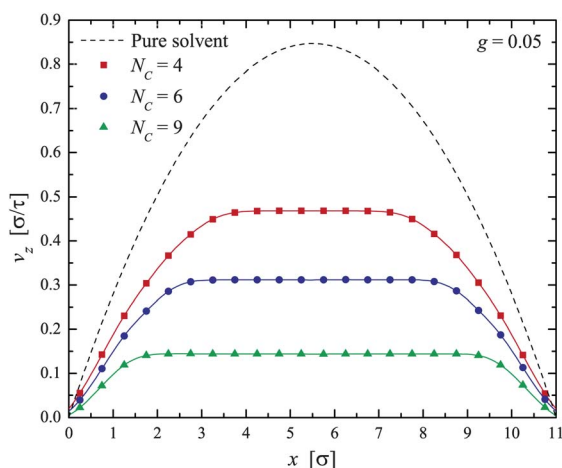
The above considerations bring forward a property of the string phase that has already been briefly addressed in ref. 55, namely that it is *global*: its stability rests on the fact that the whole, macroscopically large domain of the system forms strings but the latter cannot coexist with some other phase of different spatial symmetry in the sense of a microphase separation between the two. Thus, a different scenario emerges, in which the intact crystallinity of the central layers under Poiseuille flow causes a macroscopically thick crystalline slab to be stable within the channel. This possibility is enhanced by the fact that the solute acts back on the solvent, modifying its own velocity profile. Consequently, if such a thick chunk of crystal would flow along the fluid in the channel, then the modified solvent velocity, $v_z(x)$, would be forced, by symmetry arguments, to be flat (*i.e.*, essentially $x$-independent) far away from the walls. In such a case, the resulting local shear rate $\dot{\gamma}(x) = \partial v_z(x)/\partial x$ would be vanishingly small in that flat region, preserving the intactness of the crystalline structure. This scenario, though by no means proven on the basis of the present physical argumentation *alone*, is at least free of internal contradictions, as the preservation of the crystalline symmetry and the flatness of the solvent velocity profile are in principle consistent with one another. And though the starting point of the argument was formulated under the assumption of undistorted solvent velocity profiles, the whole *Ansatz* evidently maintains its validity in the opposite case of weak external flow.

The results of our simulations fully confirm that indeed the above scenario materializes in practice, and they offer a prime example of the ways in which the properties of the suspended particles bring about a dramatic modification of the flow properties of the pure solvent. In contrast to shear experiments,[55]
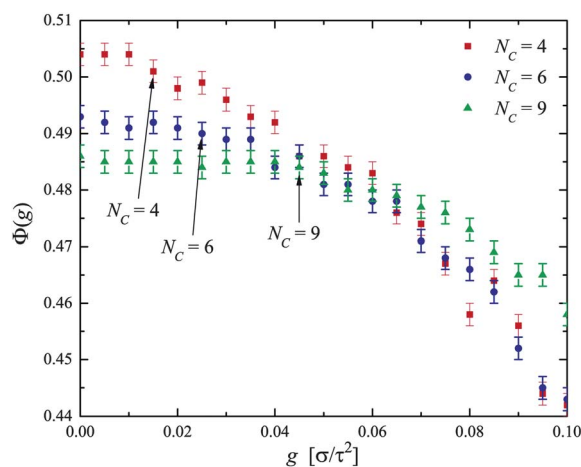
transport flow does *not* necessarily destroy the crystallographic order, but rather leads to a (slight) deformation and displacement of the crystal as a whole.

For further insight into the system's flow behavior, it is worthwhile to have a look at the velocity profile of the liquid. Fig. 6 shows $v_z(x)$, that is the flow velocity in gradient direction at $g = 0.05$. First of all, it is well visible that the velocity profile deviates strongly from the parabolic shape it would have had in the absence of the crystal; in fact, the fluid develops a profile that is very akin to *plug flow*, and which has been experimentally observed for pressure-driven flow of both intermediate-density colloidal gels[32,33] and concentrated colloidal suspensions,[37–39] including the transport through channels with spatial constrictions.[34,36,40] Moreover, the flat plateau broadens and its maximum drops with increasing particle density $\rho$, reflecting the resistance exerted by the crystal on the fluid. We can decompose this flow profile into three parts, namely two outer regions in which we find an almost linear velocity gradient, and one inner regime in which the velocity is constant. This in turn means that while an ordered slab of solute particles in the central area stream with a steady velocity, the particles closer to the walls experience considerable shear forces and hence lose their crystalline ordering.[55]

The dependence of the velocity profiles on $g$ will be analyzed in more detail in the following subsection. Here, we present further quantitative results for the behavior of the solute particles under flow. We first look at the dependence of the free volume fraction $\Phi$ on $g$; results are shown in Fig. 7. In the equilibrium state with zero flow ($g = 0$), the free volume fraction of the denser crystals is slightly lower than that of their more dilute counterparts, due to thermal fluctuations. Upon increasing $g$, the corresponding $\Phi$ values remain then constant, until they drop at a layer-melting transition, when the outermost GEM-particles are released from their initial clusters. We can readily observe that these transition points (indicated by the arrows) shift to higher $g$-values as $N_c$ is increased. Also the fact that the fluid resistance is more



**Fig. 7** Free volume fraction of the GEM particles, $\Phi(g)$ for the [100]-orientation and for different values of $N_c$, as labeled. The arrows indicate the $g$-value, at which the outermost layers melt for the first time.

pronounced for higher $N_c$ and fewer layers are liquefied is reflected in the weaker decline of the respective curves.

In order to study the crystal structure in a more quantitative fashion, we have calculated the averaged local bond order parameters, $\bar{Q}_4$ and $\bar{Q}_6$, for each density and plotted the results as a function of $g$; the results are shown in Fig. 8. The inspection of $\bar{Q}_4$ and $\bar{Q}_6$ reveals that, although the crystal is slightly deformed as a whole, its *local* structural integrity is still preserved to a high extent. Moreover, the progression of $\bar{Q}_4$ supports our finding that the less dense systems liquefy more easily, since the respective values show a distinct trend towards $\bar{Q}_4^{\text{liq}}$. This statement, however, has to be treated with caution, since the difference between the values of the parameters of the ordered and uniform system is rather small.
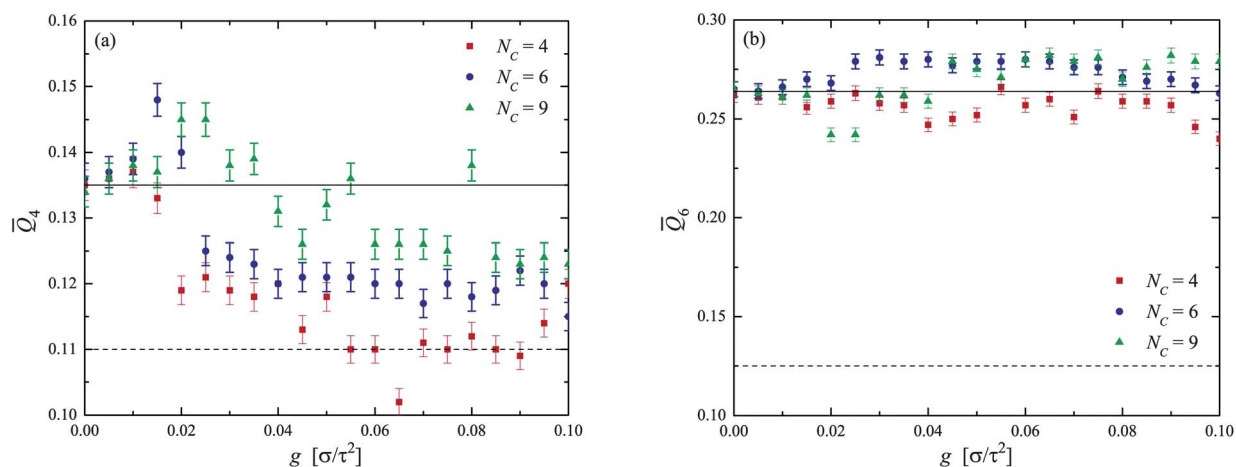
## B. Flow quantization

A more detailed analysis of the velocity profiles and their dependence on $g$ reveals a number of striking features that are unique to the cluster crystals. The plug-flow dependence of the velocity on $x$ is, of course, not a feature unique to the latter: indeed, previous experiments with both intermediate-density colloidal gels[32–34] and with concentrated colloidal suspensions[37,38,40] have resulted into flows that have very similar shapes to the representative results shown in Fig. 6. In fact, a phenomenological approach exists, which yields such plug-flows in conjunction with the Navier–Stokes equations, namely the Herschel–Bulkley model,[75] which is based on the following postulated dependence of the shear stress $\sigma_{xz}$ on the shear rate $\dot{\gamma}$:

$$\sigma_{xz} = \eta^* \dot{\gamma}^n + \sigma_0, \tag{10}$$

with the yield stress $\sigma_0$, the viscosity $\eta^*$ of the complex fluid and the shear-thinning exponent $n$.

The Herschel–Bulkley model has been applied to describe the plug-flow profiles in colloidal disordered gels.[32] In our case, the underlying physics is different, so that an attempt to describe the flux data with this model does not seem particularly



**Fig. 6** Velocity profile of the liquid in the presence of the GEM-crystal for the [100]-orientation at $g = 0.05$ and for different values of $N_c$, as labeled. The points are results from the simulation, whereas the solid lines are fits according to eqn (11). The dashed line shows the profile for the pure solvent under the same value of the external drive. The presence of the GEM particles results in a (weak) wall-slip, which decreases with $N_c$.

**Fig. 8** Bond order parameters $\bar{Q}_4$ (left panel) and $\bar{Q}_6$ (right panel) as functions of the gravitational force parameter $g$ and for different values of $N_c$, as labeled. The symbols show the data at indicated occupancy number $N_c$, while the lines represent the reference bond order parameters for the fcc arrangement (solid line) and the unordered arrangement (dashed line).

advantageous. We resort instead to an *ad hoc* fit of the velocity profiles with a function of the form:

$$v_z(x) = A \tanh(Bx) + A \tanh(B(L_x - x)) + C, \quad (11)$$

involving the fit parameters $A$, $B$ and $C$. We emphasize that there is no underlying model behind eqn (11) above; we rather employ it as a straightforward tool to extract quantitative information on three key characteristics of the plug flow, namely the height $h$ of the velocity profile, the width $w$ of its flat part and the wall-slip velocity $s$. These are readily obtainable from the fit parameters as:

$$h = 2A \tanh(BL_x/2) + C, \quad (12)$$

$$w = L_x - 2/B, \quad (13)$$

and

$$s = A \tanh(BL_x) + C. \quad (14)$$

The typical quality of the fit can be seen in Fig. 6. The results for the height, width and wall-slip of the velocity profiles are summarized in Fig. 9.

The dependence of the plateau height on $N_c$ and $g$, Fig. 9(a), reveals some remarkable novel features. First, we notice that the presence of the crystal slows down the flow, at fixed $g$, as compared to the pure solvent; this slowdown is more severe as the cluster occupancy grows, since the presence of more GEM-8 particles increases the collisions with the solvent. Second, and focusing for now on the less dense crystal, $N_c = 4$, we find the existence of a two-stage process in the flow: for sufficiently small values of $g$, the flow profile is independent of the strength of the external pressure drop, a feature akin to granular, non-Brownian matter,[36,39] whereas at higher values of $g$ the flux increases with it. Recently, Campbell and Haw[39] established a similar behavior for the flow of concentrated colloidal dispersions, in which, however, the crossover from colloidal to granular flow took place by increasing the volume fraction of the suspension. Here, the transition occurs instead at fixed concentration of the solute, and

it takes the form of a dynamical 'phase transition' with the strength of the external field $g$ as a control parameter. Even more remarkable is the evolution of these phenomena when looked upon as functions of the occupancy $N_c$. By increasing the latter, the critical value $g_c$ denoting the transition between colloidal and granular-like flow increases (see Fig. 9(a) for $N_c = 6$). Moreover, by going now to the most dense system, $N_c = 9$, a transition from the first to a second plateau is observed, and possibly even to a third. Increasing the pressure drop induced *via* $g$ leads to discrete values of the flux, separated by well-defined jumps, which are caused by successive melting of layers close to the walls. The number of melted layers can be estimated from the corresponding value of $w$. Whereas for low-occupancy crystals the melting of a layer leads to colloidal-flow behavior, for high-occupancy numbers the scenario is self-repeating after successive melting of additional layers, producing thereby a new plateau in which the flow of the system is granular-matter-like. We call this remarkable behavior *flow quantization*, and we trace its appearance in the particular nature of the cluster crystals. To the best of our knowledge, it has not yet been seen for other, common colloidal systems.

The width of the plateau, Fig. 9(b) shows the signature of flow quantization even more strongly than the plateau height. There, it can be seen that with each successive pair of molten, lubricating layers at the edges of the system, the plug-like, flat part of the profile becomes narrower, and that the width remains roughly constant until the next border layers melt. This feature, allows us to gain control not only on the strength $h$ of the flowing beam but also on its focus $w$. Finally, the wall-slip velocity $s$, Fig. 9(c), shows a constant growth with $g$ for the less dense system but it carries the signature of the discrete plateaus for the denser ones, $N_c = 6$ and $N_c = 9$. It should be kept in mind, however, that $s$ is a small number and thus prone to errors in the fitting procedure.

Fig. 10 shows the flux of solute particles $\Psi(g)$ across the simulation box, *i.e.*, the number of particles passing through the gradient–vorticity plane in unit time, and a significant dependency on $N_c$ is clearly visible. While for very small $g \lesssim 0.01$ the curves collapse onto each other, their progression differs distinctively with increasing $g$. For $N_c = 4$, $\Psi(g)$ is almost
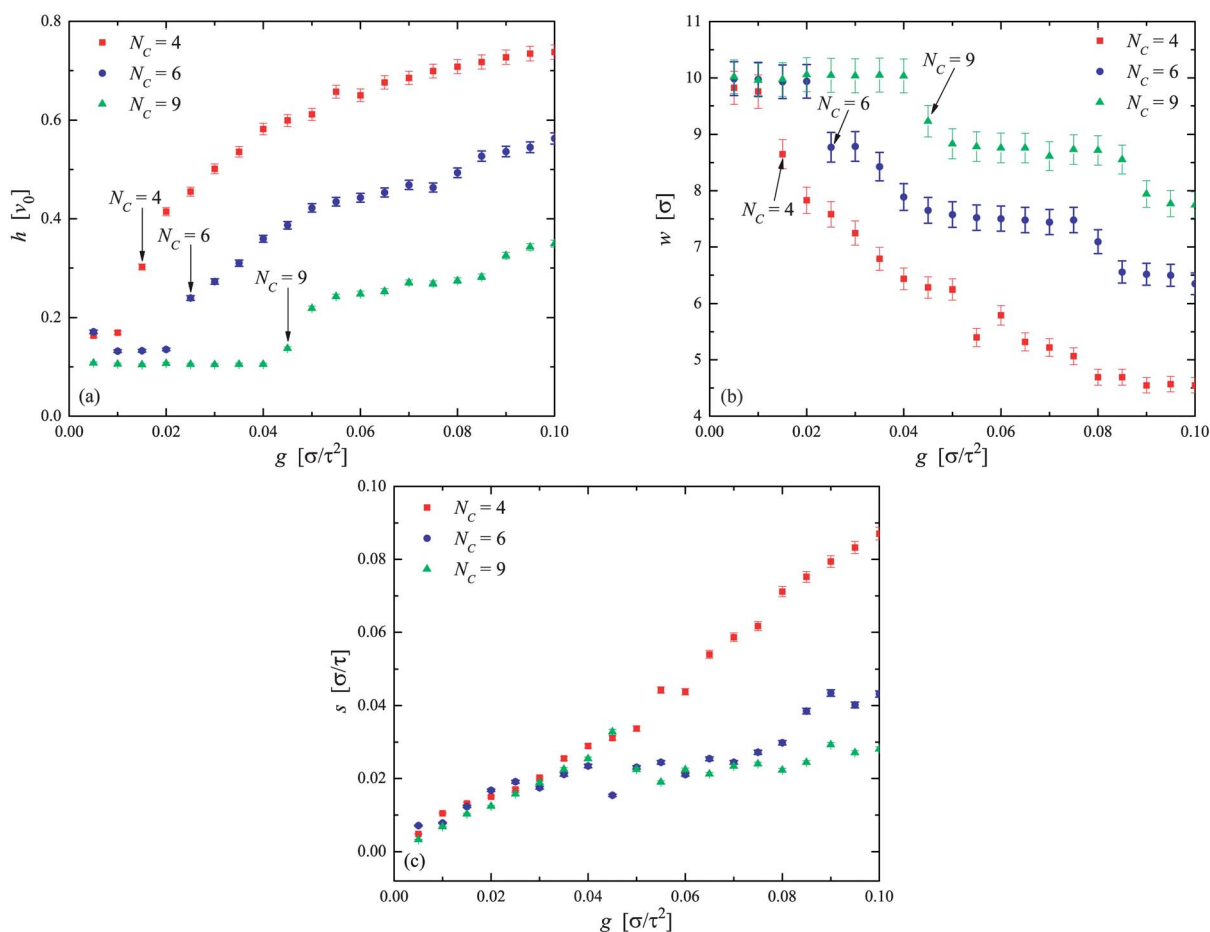
**Fig. 9** (a) The plateau height $h$ (maximum of the velocity profile) of the plug flow pattern of GEM-8 crystals driven by pressure, for crystals of different occupancy $N_c$, as a function of the magnitude of the driving force $g$. The height is expressed in units of the maximum, $v_0$, of the parabolic velocity profile in the absence of the GEM-8 particles, see eqn (8); (b) The width $w$ of the flat part of the velocity profile, for the same parameters as in (a); (c) The corresponding wall-slip velocity $s$. All results refer to a slit of width $L_x = 11\sigma$, and the positions of the arrows are the same as in Fig. 7.
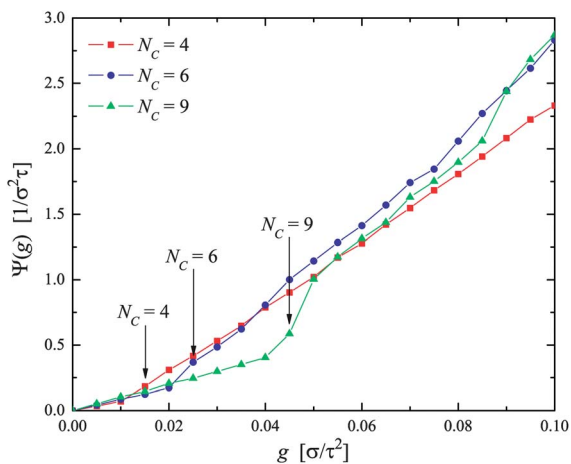


**Fig. 10** Particle flux $\Psi(g)$ as a function of the gravitational force $g$ for the [100]-orientation. The positions of the arrows are the same as in Fig. 7.

completely linear, whereas for $N_c = 6$ subtle kinks, and for $N_c = 9$ very pronounced jumps are noticeable. These non-linearities stem from the fact that with an increasing pressure gradient the crystalline layers close to the walls melt and thus reduce the drag

forces on the remaining intact lattice. Since the potential energy of the cluster crystal is proportional to the number of particles at each lattice site, the critical flow, at which the outermost layer melts for the first time, increases with $N_c$. Hence for small and intermediate $g$, the flux of the thinner systems is higher, since the liquefied layers act as a lubricant. However as $g$ is increased further, the outer layers melt in the denser systems as well, and the respective fluxes catch up and eventually overtake. Finally it is noteworthy, that the plateaus in Fig. 9(a) translate here into linear curves due to the linear dependency of $v_0$ on $g$.

All in all, both the existence of a transition from granular to colloidal flow and the presence of discrete plateaus are unique characteristics of the transport properties of cluster crystals. It is reasonable to assume that the number of plateaus will increase and the constancy of their values will become sharper for higher values of $N_c$ and also for higher widths $L_x$ of the confining channel (not studied here).

## V. Conclusions

We have presented a study of the flow properties of cluster crystals under two prototypical flow fields, namely steady shear and pressure-driven Poiseuille flow. In the former case, for which

it has already been established that these systems form string-phases, we focused on the issue of the influence that shear has on the nucleation rates of crystals out of supercooled melts. We found that the existence of the string phase under shear flow offers the system an easy pathway towards crystallization, due to the existence of partially broken spatial symmetry under shear. Once shear ceases, the further step towards full, three-dimensional symmetry breaking happens instantaneously. In this way, an effective extinction of the nucleation barrier is brought about, and an efficient way for crystallizing these soft particles opens up. As regards the transport flow, we have established some unique properties of these novel systems, which include the emergence of plug flow patterns, the corpuscular transport of an essentially undistorted crystal that 'glides' on liquefied layers on the walls, as well as the phenomenon of flow quantization on well-defined plateaus. All these characteristics have their origin in the ultra-soft, penetrable and cluster-forming nature of the $Q^{\pm}$-class of systems and they underline their highly unusual properties not only in equilibrium but also under the influence of external fields. Future work should now focus on the attempts to assemble these crystals on a microscopic basis[45] and on appropriate treatment of the dynamics of the same.

## Acknowledgements

## References

1 J. Vermant, *Curr. Opin. Colloid Interface Sci.*, 2001, **6**, 489.
2 L. V. Woodcock, *Phys. Rev. Lett.*, 1985, **54**, 1513.
3 N. J. Wagner and J. F. Brady, *Phys. Today*, 2009, **62**(10), 27.
4 B. M. Erwin, D. Vlassopoulos and M. Cloître, *J. Rheol.*, 2010, **54**, 915.
5 C. O. Osuji and D. A. Weitz, *Soft Matter*, 2008, **4**, 1388.
6 A. Chremos, K. Margaritis and A. Z. Panagiotopoulos, *Soft Matter*, 2010, **6**, 3588.
7 T. S. Davies, A. M. Ketner and S. R. Raghavan, *J. Am. Chem. Soc.*, 2006, **128**, 6669.
8 H. M. Laun, R. Bung and F. Schmidt, *J. Rheol.*, 1991, **35**, 999.
9 Y. S. Lee, E. D. Wetzel and N. J. Wagner, *J. Mater. Sci.*, 2003, **38**, 2825.
10 Y. L. Wu, D. Derks, A. van Blaaderen and A. Imhof, *Proc. Natl. Acad. Sci. U. S. A.*, 2009, **106**, 10564.
11 D. Derks, Y. L. Wu, A. van Blaaderen and A. Imhof, *Soft Matter*, 2009, **5**, 1060.
12 L. B. Chen and C. F. Zukoski, *Phys. Rev. Lett.*, 1990, **65**, 44.
13 Y. D. Yan and J. K. G. Dhont, *Phys. A*, 1993, **198**, 78.
14 L. Willner, O. Jucknischke, D. Richter, J. Roovers, L.-L. Zhou, P. M. Toporowski, L. J. Fetters, J. S. Huang, M. Y. Lin and N. Hadjichristidis, *Macromolecules*, 1994, **27**, 3821.
15 D. Vlassopoulos, G. Fytas, T. Pakula and J. Roovers, *J. Phys.: Condens. Matter*, 2001, **13**, R855.
16 G. Foffi, F. Sciortino, P. Tartaglia, F. Lo Verso, L. Reatto, K. A. Dawson and C. N. Likos, *Phys. Rev. Lett.*, 2003, **90**, 238301.
17 M. Laurati, J. Stellbrink, R. Lund, L. Willner, D. Richter and E. Zaccarelli, *Phys. Rev. Lett.*, 2005, **94**, 195504.
18 E. Stiakakis, A. Wilk, J. Kohlbrecher, D. Vlassopoulos and G. Petekidis, *Phys. Rev. E*, 2010, **81**, 020402(R).
19 K. Mortensen, W. Brown and B. Nordén, *Phys. Rev. Lett.*, 1992, **68**, 2340.
20 J. E. Smay, G. M. Gratson, R. F. Shepherd, J. Cesarano III and J. A. Lewis, *Adv. Mater.*, 2002, **14**, 1279.
21 J. E. Smay, J. Cesarano III and J. A. Lewis, *Langmuir*, 2002, **18**, 5429.
22 G.-R. Yi, T. Thorsen, V. N. Manoharan, M.-J. Hwang, S.-J. Jeon, D. J. Pine, S. R. Quake and S.-M. Yang, *Adv. Mater.*, 2003, **15**, 1300.
23 R. B. Rao, K. L. Krafcik, A. M. Morales and J. A. Lewis, *Adv. Mater.*, 2005, **17**, 289.
24 R. F. Shepherd, J. C. Conrad, S. K. Rhodes, D. R. Link, M. Marquez, D. A. Weitz and J. A. Lewis, *Langmuir*, 2006, **22**, 8618.
25 R. K. Shah, J.-W. Kim, J. J. Argesti, D. A. Weitz and L.-Y. Chu, *Soft Matter*, 2008, **4**, 2303.
26 D. Dendukuri and P. S. Doyle, *Adv. Mater.*, 2009, **21**, 1.
27 S. Seiffert and D. A. Weitz, *Soft Matter*, 2010, **6**, 3184.
28 H. Chen, J. Li, H. C. Shum, H. A. Stone and D. A. Weitz, *Soft Matter*, 2011, **7**, 2345.
29 H. M. Wyss, T. Franke, E. Mele and D. A. Weitz, *Soft Matter*, 2010, **6**, 4550.
30 A. Terray, J. Oakey and D. Marr, *Science*, 2002, **296**, 1841.
31 R. Karlsson, M. Karlsson, A. Karlsson, A.-S. Cans, J. Bergenholtz, B. Åkerman, A. G. Ewing, M. Voinova and O. Orwar, *Langmuir*, 2002, **18**, 4186.
32 M. T. Roberts, A. Mohraz, K. T. Christensen and J. A. Lewis, *Langmuir*, 2007, **23**, 8726.
33 J. C. Conrad and J. A. Lewis, *Langmuir*, 2008, **24**, 7628.
34 J. C. Conrad and J. A. Lewis, *Langmuir*, 2010, **26**, 6102.
35 H. J. Walls, S. Brett Caines, A. M. Sanchez and S. A. Khan, *J. Rheol.*, 2003, **47**, 847.
36 M. D. Haw, *Phys. Rev. Lett.*, 2004, **92**, 185506.
37 L. Isa, R. Besseling and W. Poon, *Phys. Rev. Lett.*, 2007, **98**, 198305.
38 L. Isa, R. Besseling, A. N. Morozov and W. Poon, *Phys. Rev. Lett.*, 2009, **102**, 058302.
39 A. I. Campbell and M. D. Haw, *Soft Matter*, 2010, **6**, 4688.
40 D. Genovese and J. Sparkel, *Soft Matter*, 2011, **7**, 3889.
41 S. Bastea, *Phys. Rev. E*, 2007, **75**, 031201.
42 C. Mankoc, A. Garcimartín, I. Zuriguel and D. Maza, *Phys. Rev. E*, 2009, **80**, 011309.
43 S. D. Kulkani, B. Metzger and J. F. Morris, *Phys. Rev. E*, 2010, **82**, 010402.
44 M. E. Cates, J. P. Wittmer, J.-P. Bouchaud and P. Claudin, *Phys. Rev. Lett.*, 1998, **81**, 1841.
45 B. M. Mladek, G. Kahl and C. N. Likos, *Phys. Rev. Lett.*, 2008, **100**, 028301.
46 A. Narros, A. J. Moreno and C. N. Likos, *Soft Matter*, 2010, **6**, 2435.
47 C. N. Likos, A. Lang, M. Watzlawek and H. Löwen, *Phys. Rev. E*, 2001, **63**, 031206.
48 B. M. Mladek, D. Gottwald, G. Kahl, M. Neumann and C. N. Likos, *Phys. Rev. Lett.*, 2006, **96**, 045701.
49 K. Zhang, P. Charbonneau and B. M. Mladek, *Phys. Rev. Lett.*, 2010, **105**, 245701.
50 C. N. Likos, B. M. Mladek, D. Gottwald and G. Kahl, *J. Chem. Phys.*, 2007, **126**, 224502.
51 B. M. Mladek, D. Gottwald, G. Kahl, M. Neumann and C. N. Likos, *J. Phys. Chem. B*, 2007, **111**, 12799.
52 T. Neuhaus and C. N. Likos, *J. Phys.: Condens. Matter*, 2011, **23**, 234112.
53 A. J. Moreno and C. N. Likos, *Phys. Rev. Lett.*, 2007, **99**, 107801.
54 D. Coslovich, L. Strauss and G. Kahl, *Soft Matter*, 2011, **7**, 2127.
55 A. Nikoubashman, G. Kahl and C. N. Likos, *Phys. Rev. Lett.*, 2011, **107**, 068302.
56 S. van Teeffelen, A. J. Moreno and C. N. Likos, *Soft Matter*, 2009, **5**, 1024.
57 D. A. Lenz, R. Blaak and C. N. Likos, *Soft Matter*, 2009, **5**, 2905.
58 A. Malevanets and R. Kapral, *J. Chem. Phys.*, 1999, **110**, 8605.
59 G. Gompper, T. Ihle, D. M. Kroll and R. G. Winkler, *Adv. Polym. Sci.*, 2009, **221**, 1.
60 M. Montes, A. Nikoubashman, and G. Kahl, "Hopping and diffusion of ultrasoft particles in cluster crystals in the explicit presence of a solvent," Unpublished.
61 A. Malevanets and J. M. Yeomans, *Europhys. Lett.*, 2000, **52**, 231.
62 T. Ihle and D. M. Kroll, *Phys. Rev. E*, 2001, **63**, 020201.
63 M. Hecht, J. Harting, T. Ihle and H. J. Herrmann, *Phys. Rev. E*, 2005, **72**, 011408.
64 A. W. Lees and S. F. Edwards, *J. Phys. C: Solid State Phys.*, 1972, **5**, 1921.
65 A. Nikoubashman and C. N. Likos, *Macromolecules*, 2010, **43**, 1610.
66 M. Ripoll, R. G. Winkler and G. Gompper, *Phys. Rev. Lett.*, 2006, **96**, 188302.

67 M. Hecht, J. Harting, M. Bier, J. Reinshagen and H. J. Herrmann, *Phys. Rev. E*, 2006, **74**, 021403.
68 A. Malevanets and R. Kapral, *J. Chem. Phys.*, 2000, **112**, 7260.
69 A. Lamura, G. Gompper, T. Ihle and D. M. Kroll, *Europhys. Lett.*, 2001, **56**, 319.
70 E. Allahyarov and G. Gompper, *Phys. Rev. E*, 2002, **66**, 036702.
71 A. Nikoubashman and C. N. Likos, *J. Chem. Phys.*, 2010, **133**, 074901.

72 R. Blaak, S. Auer, D. Frenkel and H. Löwen, *Phys. Rev. Lett.*, 2004, **93**, 068303.
73 P. J. Steinhardt, D. R. Nelson and M. Ronchetti, *Phys. Rev. B*, 1983, **28**, 784.
74 W. Lechner and C. Dellago, *J. Chem. Phys.*, 2008, **129**, 114707.
75 W. H. Herschel and R. Bulkley, *Kolloid-Z.*, 1926, **39**, 291.